

1 Shortening and extrusion in the East Anatolian Plateau: how was Neogene Arabia-  
2 Europe convergence tectonically accommodated?

---

3  
4 Douwe J.J. van Hinsbergen<sup>1\*</sup>, Derya Gürer<sup>2,3</sup>, Ayten Koç<sup>4</sup>, Nalan Lom<sup>1</sup>

- 5  
6 1. Department of Earth Sciences, Utrecht University, Budapestlaan 4, 3584 CD  
7 Utrecht, the Netherlands  
8 2. Research School of Earth Sciences, Australian National University, Canberra, ACT  
9 2601, Australia  
10 3. Institute of Earth Sciences, Heidelberg University, Heidelberg, 69120, Germany  
11 4. Department of Geological Engineering, Van Yüzüncü Yıl University, Van, Turkey  
12

13  
14 \*Corresponding author: [d.j.vanhinsbergen@uu.nl](mailto:d.j.vanhinsbergen@uu.nl)  
15  
16

17 **This is a non-peer reviewed manuscript, submitted for publication in Earth**  
18 **and Planetary Science Letters**  
19

## 20 Abstract

21 Deformation in orogenic belts is typically widely distributed, but may localized to  
22 form discrete, fast-moving fault zones enclosing semi-rigid microplates such as the  
23 Anatolian microplate. This plate is extruding westwards from the East Anatolian Plateau  
24 in the Arabia-Eurasia collision zone along major North and East Anatolian Faults that  
25 cause devastating earthquakes, including the February 6, 2023 East Anatolian  
26 earthquakes. However, how distributed deformation became focused, and where it may  
27 still be active is less-well understood. Here summarise the kinematic history and  
28 orogenic tectonic development that preconditioned the orogen for development of the  
29 East Anatolian Plateau and the microplate. The orogen first formed in Cretaceous to  
30 Eocene time by subduction-accretion below oceanic lithosphere preserved as ophiolites.  
31 Then, while remaining oceanic crust was subducted in late Eocene-Oligocene time, it  
32 underwent regional extension causing crystalline crust exhumation and deep-marine  
33 basin formation. From Early Miocene time onwards, during and perhaps before the  
34 onset of Arabian continental underthrusting, the plateau shortened by ~350 km,  
35 making 45 km thick crust, and causing >3 km of uplift. Microplate extrusion since the  
36 onset of North Anatolian Fault formation around 13 Ma accounted for no more than  
37 25% of Arabia-Eurasia convergence. The remaining 75% (>200 km) must thus have  
38 been accommodated by continued ~N-S shortening. We highlight that new field studies  
39 of the East Anatolian Plateau, through an integrated geological-geomorphological  
40 approach to overcome the difficulties posed by a widespread young volcanic cover, are  
41 required to identify where and how this major shortening was accommodated and to  
42 better assess seismic hazards in eastern Anatolia, and to decipher the dynamics of  
43 microplate extrusion.

44

## 45 Introduction

46 Plate tectonics describes the Earth's lithosphere as a mosaic of rigid plates that move  
47 along discrete plate boundaries (McKenzie and Parker, 1967). If plates were entirely  
48 rigid, seismicity would be strictly focused at discrete plate boundaries. However, within  
49 broadly deforming orogens fault zones focusing deformation may develop that enclose  
50 semi-rigid (micro)plates (Li et al., 2017; Mann et al., 1995; Molnar and Tapponnier,  
51 1975; Whitney et al., 2023). These fault zones pose a major seismic hazard that become

52 the focus of scientific extension. However, the identifying the regionally distributed  
53 deformation and associated hazards that precondition, and that may continue during  
54 microplate formation, is challenging.

55 The Arabia-Eurasia collision zone in eastern Anatolia is a key example of  
56 regionally distributed deformation followed by microplate formation. This Anatolian  
57 microplate is now enclosed by the North and East Anatolian transform faults that  
58 accommodate its extrusion away from the Arabia-Europe collision zone (Dewey and  
59 Şengör, 1979; Ketin, 1948) (Figure 1). This motion is associated with devastating  
60 earthquakes, including the  $M_w$  7.8 Pazarcık (Nurdağ) and  $M_w$  7.7 Ekinözü earthquakes of  
61 February 6, 2023 at the East Anatolian Fault Zone (Barbot et al., 2023; Liu et al., 2023;  
62 Melgar et al., 2023; Zhang et al., 2023). However, even though GPS measurements show  
63 that these microplate-bounding faults accommodate much of the present-day  
64 convergence of Arabia and Europe (Reilinger et al., 2006), maps of active faults (Emre et  
65 al., 2018) reveal that deformation to the east, but also within the microplate is  
66 widespread and distributed across faults with isolated surface ruptures that do not  
67 make a coherent fault mosaic.

68 The earthquakes of 2023 placed understanding the dynamics of eastern  
69 Anatolian deformation once again in the center of scientific attention. Whereas the  
70 extrusion-accommodating microplate boundaries receive – logically – most attention,  
71 we here focus on the possible role that distributed deformation may have on adding  
72 seismic hazard, and what information it may hold about microplate evolution and  
73 dynamics. To this end, we here summarize the architecture and history of the east  
74 Anatolian plateau, starting at the beginning of its orogenic history. The Anatolian  
75 microplate started forming only ~13 Ma ago, within a regionally deformed orogenic belt  
76 that experienced more than 100 Ma of accretionary orogenesis and re-deformation by  
77 upper plate extension and shortening (van Hinsbergen et al., 2020) (Figure 1). This  
78 orogenesis accommodated more than 2000 km of plate convergence, of which  
79 surprisingly little has so far been recognized as shortening in the field. This may be in  
80 part because of wholesale lithospheric subduction (Gürer and van Hinsbergen, 2019),  
81 but likely also because shortening has not been the focus of attention.

82 In this paper, we first summarize the orogenic evolution of the East Anatolian  
83 Orogen that preconditioned plateau rise and microplate formation based on the recent  
84 detailed regional kinematic restoration of Mediterranean tectonics of (van Hinsbergen

85 et al., 2020). We then explain the available structural geological and paleomagnetic data  
86 that allows reconstruction of microplate motion. We will estimate the role of shortening  
87 that must have occurred during microplate development by comparing the amount of  
88 convergence required to restore Anatolian extrusion with the total amount of  
89 convergence. We will then evaluate how and where the remaining convergence may  
90 have been accommodated, and what role shortening may have played in driving  
91 initiation and evolution of East Anatolian Plateau rise, microplate formation, and  
92 extrusion. Finally, we identify targets for future field research required to assess seismic  
93 hazards associated with distributed deformation in the east Anatolian orogenic belt in  
94 addition to the major North and East Anatolian transform faults.

95

## 96 Regional plate tectonic setting and subduction history

97 The Anatolian orogen formed because of continental and oceanic subduction at  
98 multiple subduction plate boundaries that accommodated convergence between Africa-  
99 Arabia and Eurasia since the Mesozoic. The North and East Anatolian faults that  
100 delineate the modern Anatolian microplate are relatively young structures, which cut  
101 through that older orogenic belt (Figure 2). We here summarize the history of  
102 subduction and orogenesis for the eastern Anatolian part of the system, and refer the  
103 reader for a more detailed account of the plate kinematic setting, orogenic architecture,  
104 and regional context of Mediterranean tectonics to van Hinsbergen et al. (2020).

105 The eastern Anatolian orogen is the highest part of the mountain belt, with an  
106 average elevation of 2 km and peaks well over 3 km. It is supported by a thick crust of  
107 45 km thick, but only a thin mantle lithosphere (Barazangi et al., 2006; Zor et al., 2003).  
108 This plateau is widely covered by young volcanics (Keskin, 2003), but below these,  
109 crystalline and non-crystalline nappes, ophiolites, plutons, and Cenozoic sedimentary  
110 basins and volcanics are exposed that allow correlation to better-exposed and better-  
111 studied orogenic architecture to the west (Figure 3).

112 The Pontides-Lesser Caucasus fold-thrust belt of northern Turkey and Armenia  
113 formed the southern active margin of Eurasia since Jurassic time and were located  
114 north of a north-dipping subduction zone and south of associated back-arc basins  
115 (Şengör and Yılmaz, 1981; van Hinsbergen et al., 2020). The latter include the Black Sea  
116 basins that still exist today and the Greater Caucasus Basin that was since the late



117 Eocene consumed by a small subduction zone forming the Caucasus fold-thrust belt  
118 (Cowgill et al., 2016). Caucasus shortening accounted for ~30% of the Arabia-Eurasia  
119 convergence since the Oligocene, i.e., some 250 km (Cowgill et al., 2016). It gradually  
120 decreased west- and eastward, causing northward convex oroclinal bending that also  
121 affected the eastern Anatolian orogen to the south (van der Boon et al., 2018). South of  
122 the Lesser Caucasus Block, a small continental fragment, the South Armenian Block  
123 collided with the Lesser Caucasus in the Late Cretaceous (Nikogosian et al., 2023;  
124 Sosson et al., 2010), after which subduction transferred to its south, within  
125 northeastern Anatolia (van Hinsbergen et al., 2020).

126         The Pontides and the South Armenian Block are bounded to the south by the  
127 Izmir-Ankara Suture zone and the Kağızman-Khoy Suture, respectively, from the  
128 eastern Tauride fold-thrust belt (Figures 1 and 2). The Tauride fold thrust belt underlies  
129 most of eastern Anatolia up to and including the Bitlis Mountains and is in eastern  
130 Turkey almost everywhere metamorphosed (Küşçü et al., 2010; Oberhänsli et al., 2014;  
131 Topuz et al., 2017). The eastern Tauride fold-thrust belt is separated from the Arabian  
132 continent by the Bitlis Suture (Figure 1). The Taurides contain thrust remains of the  
133 continental crust of the 'Greater Adria' microcontinental realm that continued  
134 westwards to the circum-Adriatic region of the Central Mediterranean region (van  
135 Hinsbergen et al., 2020). This continental crust was separated from Eurasia and Africa-  
136 Arabia by a northern and southern Neotethyan oceanic branch, respectively, within  
137 which intra-oceanic subduction occurred in the Late Cretaceous, and remains of which  
138 are found as ophiolites. These ophiolites and underlying mélanges now form the highest  
139 structural units of the Tauride fold-thrust belt, and were also thrust southwards onto  
140 the Arabian continental margin (Robertson et al., 2007; see detailed review and  
141 reconstruction in Maffione et al., 2017; van Hinsbergen et al., 2020) (Figure 3).

142         The closure of the northern Neotethys Ocean between the Taurides and Pontides  
143 was diachronous, younging eastwards throughout Turkey (van Hinsbergen et al., 2020).  
144 In central and western Anatolia, closure occurred in latest Cretaceous to Paleocene time  
145 (Mueller et al., 2019; Ocakoğlu et al., 2019) and Africa-Eurasia convergence was  
146 accommodated at the Cyprus trench where in the late Miocene (~9 Ma) the first  
147 continental crust of the North African margin arrived (McPhee and van Hinsbergen,  
148 2019). In the eastern Anatolia, however, convergence between the Taurides and  
149 Pontides continued into the late Miocene, as shown by extensive terrestrial and marine

150 sedimentation in the Sivas foreland basin until that time (Legeay et al., 2019). This  
151 convergence accommodated a paleomagnetically documented regional  
152 counterclockwise rotation of  $\sim 30^\circ$  of the eastern southern and eastern Tauride Orogen  
153 since the latest Oligocene-early Miocene,  $\sim 25$ -20 Ma (Cinku, 2017; Cinku et al., 2017;  
154 Gürer and van Hinsbergen, 2019; Gürer et al., 2018). Convergence and shortening  
155 between the eastern Taurides and Pontides must have continued until the poorly  
156 known arrest of rotation. The youngest documented shortening in the Sivas Basin is  
157 Late Miocene in age, but demonstrated shortening magnitudes are on the order of only a  
158 few tens of km (Legeay et al., 2019), much less than contemporaneous convergence  
159 (Gürer and van Hinsbergen, 2019).

160 Simultaneously with the Cenozoic closure of the northern oceanic branch, i.e., the  
161 Neotethyan Ocean, also a southern Eastern Mediterranean oceanic branch was closed at  
162 the Bitlis subduction zone (Fig 2). The Tauride accretionary orogen was located in the  
163 upper plate of the north-dipping Bitlis subduction zone and was during this time  
164 intruded by a widely distributed volcanic arc (Küşçü et al., 2010; 2013). In latest  
165 Cretaceous to middle Eocene time, the eastern Tauride orogen underwent regional  
166 extension (Figure 3). Deep, crystalline portions of the orogen and arc were exhumed  
167 and overlain by Lower to Middle Eocene terrestrial, volcanic, and marine sediments  
168 (Küşçü et al., 2013). In the south of the orogen, in the forearc above the Bitlis  
169 subduction zone, the deep-marine Maden and Hakkari basins formed (Aktaş and  
170 Robertson, 1984; Robertson et al., 2007). Extension continued into the Oligocene, e.g., in  
171 the Muş Basin (Hüsing et al., 2009)). These basins became shortened and thrustured since  
172 the late Oligocene (Aktaş and Robertson, 1984; Hüsing et al., 2009) and throughout the  
173 Miocene (Koçyiğit et al., 2001; Yusufoglu, 2013). The onset of shortening predates the  
174 final closure of this southern branch in eastern Anatolia that occurred with the arrival of  
175 the northern Arabian margin at the Bitlis subduction zone in early to middle Miocene  
176 time,  $\sim 18$  Ma (Figure 3; see next section).

177 In summary, the eastern Anatolian orogenic crust experienced distributed,  
178 intense, and polyphase deformation in response to accretion and the  
179 closure/termination of multiple subduction systems (Figure 3). When these subduction  
180 zones ceased, and whether this process was diachronous is poorly constrained. Within  
181 this complex orogenic collage, the North and East Anatolian Faults started forming in  
182 late Miocene time, to eventually delineate the Anatolian microplate.

## 184 Neogene deformation in eastern Anatolia

185 To reconstruct how the extruding Anatolian microplate developed in the East  
186 Anatolian Plateau, we first review the available, but sparse, constraints on Neogene fault  
187 displacements in eastern Anatolia. Next, we reconstruct these faults in the context of  
188 regional plate motion. The amount and rate of Africa-Arabia-Eurasia convergence are  
189 determined from reconstructions of a plate circuit made by reconstructing the North  
190 and Central Atlantic oceans and the Red Sea basin, which in late Neogene time has  
191 uncertainties of only a few percent (e.g., DeMets et al., 2015; DeMets and Merkouriev,  
192 2016). For the reconstruction of the Caucasus orocline, we adopt the reconstruction of  
193 van der Boon et al. (2018), and for the long-term evolution of Anatolia since the  
194 Mesozoic, we use the reconstruction of Mediterranean orogenic belts of van Hinsbergen  
195 et al. (2020).

196 The present-day Anatolian microplate is separated from the Eurasian Plate by the  
197 dextral North Anatolian Fault Zone to the Karlıova ‘triple junction’ (Sengör, 1979),  
198 where it merges with the Varto Fault Zone, a thrust system, and the East Anatolian Fault  
199 Zone (Karaoğlu et al., 2017; Sançar et al., 2015) (Figures 3 and 4). The East Anatolian  
200 Fault Zone ends to the southwest in the Amik (or Hatay) Triple Junction where it meets  
201 the Cyprus Trench that separates Anatolia and Africa, and the Dead Sea transform fault  
202 that separates Africa from Arabia (Duman and Emre, 2013; Tarı et al., 2013) (Figures 3  
203 and 4). However, the Anatolian micro-‘plate’, as well as the southern Eurasian margin,  
204 are not rigid. Active fault zones within the Anatolian microplate include the Faults that  
205 branch southward off the North Anatolian Fault and the Malatya-Ovacık Fault (Figure  
206 1), although their motions are subordinate to the North and East Anatolian Faults (Emre  
207 et al., 2018; Higgins et al., 2015; Koçyiğit and Beyhan, 1998). The westward decreasing  
208 Caucasus shortening also affects the southern Eurasian margin to the north of the  
209 eastern part of the North Anatolian Fault (Simão et al., 2016).

210 The onset age of formation of the 1400 km long North Anatolian Fault Zone is  
211 estimated from terrestrial stratigraphy in transtensional basins at ~13-11 Ma (Şengör  
212 et al., 2005). U/Pb dating of calcite fabrics from the North Anatolian Fault zone in  
213 central and western Anatolia yielded an age of 11 Ma age (Nuriel et al., 2019). However,  
214 whether the North Anatolian Fault Zone formed along its entire modern length

215 simultaneously is debated: evidence from basins and offset markers in the western  
216 portion of the fault zone has been used to argue for a westward propagation of the fault  
217 zone, reaching the Aegean domain only in Pliocene time (Racano et al., 2023;  
218 Sakellariou and Tsampouraki-Kraounaki, 2019; Şengör et al., 2005). The total offset of  
219 the North Anatolian Fault Zone has been estimated at up to 85 km (Akbayram et al.,  
220 2016; Hubert-Ferrari et al., 2002; Şengör et al., 2005), although reconstructions of the  
221 Aegean region account for only some tens of km of motion (van Hinsbergen et al., 2006).  
222 Perhaps some tens of km (Hubert-Ferrari et al., 2009), may thus have been  
223 accommodated within central or western Anatolia, although where and how remains  
224 poorly known (van Hinsbergen et al., 2020). In our discussions, we use a total amount of  
225 85 km right-lateral slip along the North Anatolian Fault Zone as a maximum  
226 displacement estimate, since 13 Ma.

227         The Karlıova Triple Junction at the eastern termination of the North Anatolian  
228 Fault is a transform-transform-thrust triple junction that migrates WNW-ward along  
229 the North Anatolian Fault. To the east of the Karlıova Triple Junction, the Varto Fault  
230 Zone has a similar orientation as the North Anatolian Fault (Figures 3 and 4). Currently,  
231 it is a seismically active thrust zone that accommodates part of the Arabia-Eurasia  
232 convergence (Sançar et al., 2015). Horizontal striations on fault surfaces show that it  
233 was indeed a strike-slip fault zone in the past, when the triple junction was located  
234 farther to the east (Karaoğlu et al., 2017). The exposed length of the fault zone is 35 km  
235 providing a minimum westward migration of the Karlıova Triple Junction since the  
236 formation of the East Anatolian Fault Zone, but its eastward continuation may be buried  
237 below young volcanics (Figure 3). There is no estimate for the N-S shortening that was  
238 accommodated by the Varto Fault Zone, but it cannot have accommodated more than a  
239 small portion of the late Neogene Arabia-Eurasia convergence. This is illustrated by the  
240 numerous active E-W trending thrust faults that have been mapped between the Bitlis  
241 suture zone in the south and the Caucasus in the north (Emre et al., 2018; Koçyiğit et al.,  
242 2001). However, these faults are laterally discontinuous at the surface, suggesting they  
243 are mostly blind, buried below young volcanics. They are widely distributed from the  
244 Caucasus to the Bitlis Suture, and their cumulative displacement since the Miocene has  
245 not been estimated previously.

246         The age of the East Anatolian Fault Zone is estimated to be much younger than for  
247 the North Anatolian Fault Zone: only 6-3 Ma. These estimates are indirect at best: they

248 are based on an assumed link between 6 Ma volcanism and deformation in the Karlıova  
249 Triple Junction region (Karaoğlu et al., 2017), the interpretation that 5 Ma thermal  
250 resetting of fission track ages along the fault zone results from fluids assuming that  
251 these fluids mark the onset of the East Anatolian Fault (Whitney et al., 2023), and the  
252 ages of displaced volcanic and sedimentary rocks (Westaway and Arger, 2001). Perhaps  
253 the most direct/robust age indication comes from the Elbistan Basin that is located just  
254 north of the Sürgü Fault (Yusufoğlu, 2013). This basin is an Early Pliocene terrestrial  
255 pull-apart basin between left-lateral strike-slip faults that formed in folded Lower to  
256 Upper Miocene marine sediments. These observations record a regional change from  
257 contractional deformation to strike-slip-dominated deformation around the beginning  
258 of the Pliocene, i.e. ~5 Ma (Yusufoğlu, 2013). This is consistent with observations across  
259 the east Anatolian plateau, where Miocene strata are folded, but upper Pliocene and  
260 younger volcanic rocks that are widespread in the region, are not (Koçyiğit et al., 2001).  
261 Offset markers showed between ~15 and 27 km of total displacement of the East  
262 Anatolian Fault Zone (Saroğlu, 1992; Yönlü et al., 2013). The E-W oriented Sürgü Fault,  
263 along which the  $M_w$  7.7 2023 Ekinözü earthquake occurred (Liu et al., 2023),  
264 particularly its E-W segment (Figures 3 and 4), functions as a left lateral strike-slip fault  
265 with reverse component (Balkaya et al., 2021; Duman et al., 2020; Koç and Kaymakçı,  
266 2013). The fault connects westward to the Yakapınar-Göksun Fault that transfers its slip  
267 towards the Cyprus trench (Koç and Kaymakçı, 2013; Westaway, 2004). The Sürgü Fault  
268 is taking up approximately one third of the total plate boundary slip in recent times and  
269 prior to the Pliocene it acted as thrust fault with a dextral component that  
270 accommodated part of the Arabia-Eurasia convergence (Koç and Kaymakçı, 2013).

271 If the East Anatolian Fault did not exist until ~6-5 Ma, the Arabia-Anatolia plate  
272 boundary must have been located farther west before this time (Kaymakçı et al., 2010;  
273 Westaway and Arger, 2001). Candidate fault zones are NE-SW trending faults inferred  
274 from mapped, abrupt discontinuities in the Taurides fold-thrust belt (Kaymakçı et al.,  
275 2010), including the Göksün and Malatya-Ovacık Faults (Figure 2). Only the latter of  
276 these has been studied in detail in the field. The Malatya-Ovacık Fault is still seismically  
277 active and accommodates 2-3 mm/a of left-lateral motion (Sançar et al., 2019; 2020).  
278 Field studies have shown that between 5 and 3 Ma, it accommodated a left-lateral  
279 displacement of ~29 km (Westaway and Arger, 2001). The Malatya-Ovacık Basin had  
280 already formed by transtension in Early to Mid-Miocene time (Kaymakçı et al., 2010),

281 but there is no estimate of pre-Pliocene fault displacements. A roughly estimated a  
282 minimum of 20 km of displacement of the NNE-SSW trending Göksün Fault (not to be  
283 confused with the Yakapınar-Göksun Fault, Figure 3) that cuts through the eastern  
284 Taurides was estimated based on the horizontal offset of mapped units (van Hinsbergen  
285 et al., 2020), but no detailed field study has been performed to corroborate apparent  
286 horizontal displacement. Farther west, the Ecemiş Fault is a prominent structure that  
287 transferred Arabia/Africa-Europe convergence to the Sivas Basin region and culminated  
288 in a displacement of the Tauride fold-thrust belt of 60-80 km (Gürer et al., 2016; Jaffey  
289 and Robertson, 2001). However, the Ecemiş Fault is sealed in the south by Lower  
290 Miocene sediments, and after the Early Miocene, it only accommodated minor E-W  
291 extension (Gürer et al., 2016; Higgins et al., 2015): it therefore did not play a significant  
292 role in the development of the Anatolian microplate.

293 During the Miocene, the Bitlis Massif thrust over the Arabian continental  
294 margin, as well as onto ophiolites that were obducted onto that margin in the Late  
295 Cretaceous (Oberhänsli et al., 2010). These overthrust ophiolites are exposed in a  
296 window 40 km north of the Bitlis thrust front, providing a minimum amount for the  
297 Miocene thrust displacement (Oberhänsli et al., 2010; Yılmaz et al., 1981). Low-  
298 temperature thermochronology revealed cooling ages of the Bitlis Massif between ~18  
299 and 13 Ma (Cavazza et al., 2018; Okay et al., 2010). The Muş Basin that overlies the  
300 massif was uplifted in the middle Miocene (Huvaz, 2009), and sedimentary successions  
301 overlying the northeastern margin of the Bitlis Massif were uplifted from deep-marine  
302 to terrestrial conditions between 19 and 17 Ma (Gülyüz et al., 2020). This suggests that  
303 the Arabian continental margin first began to underthrust the Bitlis Massif around 19-  
304 18 Ma, and continued to do so until at least ~13 Ma. However, a 6 km thick pile of deep-  
305 marine turbidites in the Kahramanmaraş Basin, located on the northwestern margin of  
306 Arabia (Figure 3) and overthrust by the eastern Tauride orogen, formed later,  
307 between 13-11 Ma (Hüsing et al., 2009) showing that the thrusting of the eastern  
308 Tauride orogen over the Arabian margin became younger to the west. There is currently  
309 no geological evidence that Arabian underthrusting below the Bitlis Massif must have  
310 continued after 11 Ma. At present, the faults between the Bitlis Massif and Arabia  
311 display limited seismicity (Tan et al., 2008) (Figure 4).

312

## 313 Reconstruction

314 We now use the plate circuit and the known fault displacements and ages  
315 summarized above to evaluate how much Arabia-Eurasia convergence was  
316 accommodated by westward block extrusion away from the collision zone and where  
317 else Arabia-Eurasia convergence may have been accommodated within the east  
318 Anatolian orogen. Following this, we will assess the implications of these  
319 reconstructions for understanding the dynamics driving rise of the East Anatolian  
320 Plateau and the onset of extrusion, as well as for evaluating seismic hazards in eastern  
321 Anatolia.

322 The plate circuit reveals that Arabia-Eurasia convergence has been  $\sim 2$  cm/a  
323 throughout the Neogene. The youngest known age for the activity of the Bitlis Suture  
324 Zone of  $\sim 11$  Ma (Cavazza et al., 2018; Faccenna et al., 2006; Hüsing et al., 2009; Okay et  
325 al., 2010; Şengör et al., 2003) coincides with the estimates for the onset of North  
326 Anatolian Fault activity at 13-11 Ma (Nuriel et al., 2019; Şengör et al., 2005) and the 13-  
327 11 Ma age estimate based on a magmatic flareup for the age of slab break-off (Keskin,  
328 2003). We therefore first evaluate whether this time coincides with an abrupt change  
329 from subduction to extrusion, such that Anatolian extrusion may have accommodated  
330 all post-11-13 Ma Arabia-Eurasia convergence. To this end, we simplify the geometry of  
331 Anatolia to a schematic North and East Anatolian Fault and ignore the reality that the  
332 Arabia-Anatolia plate boundary prior to  $\sim 5-6$  Ma was likely located or distributed at  
333 faults farther west (Figure 5). We will add this complexity to our analysis later.

334 The Eurasia-North America-Africa-Arabia plate circuit shows that since the 13 Ma  
335 onset of formation of the North Anatolian Fault,  $\sim 270$  km of NNW-SSE convergence was  
336 accommodated at a location coinciding with the Karlova Triple Junction (Figure 5). To  
337 accommodate all this convergence with extrusion, the wedge-shaped microplate  
338 defined by the North and East Anatolian faults, would need to be restored 375 km  
339 eastwards along the North Anatolian Fault at 13 Ma (Figure 5). This is a far greater  
340 displacement than even the maximum field-based estimate of 85 km (Akbayram et al.,  
341 2016; Hubert-Ferrari et al., 2002; Şengör et al., 2005). Restoring this maximum  
342 displacement estimate for the North Anatolian Fault instead reveals that no more than  
343  $\sim 65$  km of NNW-SSE Arabia-Eurasia convergence has been accommodated by westward  
344 extrusion (Figure 5). This means that since the onset of formation of the North  
345 Anatolian Fault,  $>200$  km of Arabia-Europe convergence must have been accommodated

346 by shortening elsewhere in the eastern Anatolian orogen, to the south and/or north of  
347 the North and East Anatolian Faults.

348

## 349 Discussion

350 Our reconstruction shows that the amount of Anatolian extrusion since the  
351 formation of the North Anatolia Fault Zone around 13-11 Ma cannot account for  
352 contemporaneous Arabia-Eurasia convergence in eastern Anatolia. If this was the case,  
353 the displacement of the North Anatolian fault has been grossly underestimated by  
354 hundreds of kilometers (Figure 5). From this, we infer that throughout much of the  
355 extrusion history, the eastern Anatolian orogen must have been shortened by ~200 km  
356 and the extrusion-accommodating transform faults must have developed within a  
357 deforming orogenic belt (Figure 5). Because at the present-day, extrusion is more or  
358 less balancing Arabia-Eurasia convergence west of the Karlıova Triple Junction  
359 (Reilinger et al., 2006), extrusion must have accelerated through time. This is consistent  
360 with evidence that the onset of slip on the North Anatolian Fault becomes younger along  
361 the fault zone, only reaching the strands in western Anatolia in the Pliocene (Hubert-  
362 Ferrari et al., 2009; Racano et al., 2023; Şengör et al., 2005). Consequently, pre-Pliocene  
363 strike-slip displacements must have been accommodated within central Anatolia, but  
364 where and how is poorly known: major structures such as the Ecemiş Fault and the  
365 enigmatic Central Anatolian Fault zone that runs through the Sivas Basin have little  
366 post-Early Miocene displacement (Gürer et al., 2016; Jaffey and Robertson, 2001;  
367 Koçyiğit and Beyhan, 1998). The absence of major deformed belts within Central  
368 Anatolia that could accommodate North Anatolian Fault displacement suggests that pre-  
369 Pliocene motion was indeed limited and that particularly for the late Miocene, but also  
370 in the Plio-Pleistocene, Arabia-Eurasia convergence in eastern Anatolia must mostly  
371 have been accommodated by shortening, marking a 'transition period' (Koçyiğit et al.,  
372 2001) between the onset of extrusion-accommodating strike-slip fault formation and  
373 the establishment of the present-day Anatolian 'microplate'.

374 Finding where this late Miocene and younger shortening component of ~200 km  
375 was accommodated is not straightforward. To illustrate, this is a similar amount of  
376 shortening as reconstructing from the Pyrenees (Muñoz, 1992) or the southern Andes  
377 (Schepers et al., 2017). In the youngest major thrust zones that could have localized



378 such convergence, the Sivas Basin or the Bitlis Suture Zone, no major late Miocene and  
379 younger shortening has so far been recognized (Hüsing et al., 2009; Legeay et al., 2019),  
380 but paleomagnetic data attest to large-scale orogenic deformation since the middle  
381 Miocene.

382 We may use paleomagnetic rotations of the pre-Neogene Tauride Orogen as a  
383 marker to assess how the 'missing' convergence was distributed over the orogen.  
384 Paleomagnetic evidence from the eastern Tauride Orogen from central to far-eastern  
385 Anatolia revealed a coherent,  $\sim 30^\circ$  counterclockwise vertical axis rotation since the late  
386 Oligocene-early Miocene,  $\sim 25$ -20 Ma (Cinku, 2017; Cinku et al., 2017; Gürer et al.,  
387 2018). Reconstructing such a rotation around a rotation pole marked by an oroclinal  
388 recognized in central Anatolia (Gürer and van Hinsbergen, 2019; Lefebvre et al., 2013)  
389 allows to keep the Bitlis massif attached to the north Arabian margin in the late Early to  
390 Middle Miocene, consistent with the estimated collision age from geological  
391 reconstructions (Cavazza et al., 2018; Okay et al., 2010), while at the same time  
392 maintaining the connection of the eastern Taurides to Central Anatolia (Gürer and van  
393 Hinsbergen, 2019; van Hinsbergen et al., 2020) (Figure 6). This rotation also predicts  
394 that the onset of thrusting of the eastern Tauride orogen over the Arabian continental  
395 margin was diachronous, becoming younger westwards, consistent with the  
396 observations from Kahramanmaraş. Restoring the full  $30^\circ$  rotation since the Oligocene  
397 however, requires that shortening between the eastern Taurides and eastern Pontides  
398 started before the collision of Arabia with the eastern Taurides (Bitlis) massif,  
399 consistent with evidence for Oligocene shortening in the Sivas Basin (Legeay et al.,  
400 2019). This rotational deformation of the eastern Taurides suggests that post-Early  
401 Miocene shortening to the north of the Tauride Orogen (i.e., in central Sivas Basin region  
402 (Gürer et al., 2018)) increases eastwards, and the amount of post-Early Miocene  
403 convergence accommodated by the Cyprus trench and Bitlis Suture Zone decreases  
404 eastwards (Figure 6).

405 We may further constrain the distribution of shortening by estimating  
406 displacements of the strike-slip faults that cut the Tauride Orogen. For instance, the left-  
407 lateral displacement of the Malatya-Ovacik fault zone between 5 and 3 Ma transferred  
408 an estimated 28 km of convergence from the south to the north of the Tauride Orogen  
409 (Westaway and Arger, 2001). Determining the timing and amount of displacement of  
410 the other strike-slip faults and associated basins cutting through the eastern Taurides,

411 mapped by Kaymakcı et al. (2010), such as the Göksün Fault (Figure 3) may thus  
412 identify further where the shortening was partitioned over the Sivas basin and its  
413 eastern continuation, or the Bitlis Suture Zone.

414 The recognition that extrusion was likely an accelerating process, gradually taking  
415 an increasing component of the convergence may shed light on the potential triggers for  
416 extrusion. Often-quoted causes point at tectonic stresses caused by Arabia-Eurasia  
417 convergence, combined with a westward gradient caused by excess gravitational  
418 potential energy, and perhaps associated mantle flow, due to East Anatolian Plateau rise  
419 in the east combined with Aegean extension and subsidence in the west (Faccenna et al.,  
420 2006; Le Pichon and Kreemer, 2010; Sternai et al., 2014; Whitney et al., 2023). Aegean  
421 extension started well before extrusion, around 45 Ma, and accelerated around 25 and  
422 15 Ma (Brun and Sokoutis, 2010; Philippon et al., 2014; van Hinsbergen and Schmid,  
423 2012). Hence, this extension may have preconditioned westward extrusion, but its  
424 onset or development does not provide an obvious trigger for the extrusion. The rise of  
425 the East Anatolian Plateau coincides closer with the onset of extrusion: when the North  
426 Anatolian Fault started to form in the middle Miocene, marine sedimentation still  
427 occurred in regions that are now uplifted by a kilometer or more (e.g., in the Sivas Basin  
428 and its eastern continuation (Legeay et al., 2019; Şengör et al., 2003)). Plateau rise in  
429 general may have several causes, including crustal shortening and thickening,  
430 continental underthrusting, or dynamic topographic rise due to slab break-off or  
431 various ways of mantle lithospheric delamination (Göğüş and Pysklywec, 2008; Keskin,  
432 2003; Memiş et al., 2020; Şengör et al., 2003) and these processes may all contribute at  
433 different times and locations, as they likely did in Central Anatolia (McPhee et al., 2022).  
434 For eastern Anatolia, dynamic topographic rise has so far favored the interpretation  
435 (Faccenna et al., 2006; Keskin, 2003; Memiş et al., 2020; Molin et al., 2023; Şengör et al.,  
436 2003; Whitney et al., 2023). For instance, seismic tomographic evidence shows a broken  
437 off 'Bitlis' slab in the upper mantle below the northern Arabian margin in eastern  
438 Anatolia (Faccenna et al., 2006; Hafkenscheid et al., 2006). A middle Miocene volcanic  
439 flareup in the East Anatolian Plateau may date that event at 13-11 Ma (Keskin, 2003)  
440 and slab break-off may thus have contributed to early topographic rise, but the effects  
441 are typically limited to the region directly above the breaking slab, not the entire upper  
442 plate plateau (Buitter et al., 2002).

443 Another possible cause for uplift is the underthrusting of buoyant continental  
444 crust (e.g., Kapp and Guynn, 2004; van Hinsbergen, 2022). Following slab break-off,  
445 horizontal underthrusting of Arabian lithosphere occurred: seismological observation  
446 suggest that it currently protrudes  $100 \pm 50$  km below eastern Anatolia (Whitney et al.,  
447 2023). Whitney et al. (2023) postulated that horizontal Arabian underthrusting below  
448 the orogen started 5 Ma ago and triggered the formation of the East Anatolian Fault and  
449 thereby established a rigid Anatolian microplate. However, this hypothesis would  
450 require that all post-5 Ma Arabia-Eurasia convergence was accommodated by Arabian  
451 underthrusting below the Bitlis massif, whereas there is no evidence that thrusting  
452 south of the Bitlis occurred after 11 Ma. Moreover, geological reconstructions and GPS  
453 motions reveal that a large part of Pliocene Arabia-Eurasia convergence was  
454 accommodated in the Caucasus (Cowgill et al., 2016; van der Boon et al., 2018). The  
455 horizontal underthrusting of Arabia below the eastern Tauride orogen must thus be  
456 older and likely occurred in the period directly following upon slab break-off. Hence,  
457 while it may have contributed to uplifting the southern part of the East Anatolian  
458 Plateau, it is not a likely trigger for East Anatolian Fault formation and is not likely to be  
459 a sole trigger for extrusion.

460 The seismological observations showing 45 km thick crust but only a thin mantle  
461 lithosphere (Barazangi et al., 2006) led to arguments that lithosphere removal could  
462 have caused rapid topographic rise since the Middle Miocene (Şengör et al., 2003)  
463 Mechanisms for delamination of a hypothetical mantle lithosphere below the East  
464 Anatolian plateau were later explored through numerical modeling (Göğüş and  
465 Pysklywec, 2008; Memiş et al., 2020). However, in the light of the longer orogenic  
466 history, the availability of a thick mantle lithosphere to delaminate in the Miocene is  
467 questionable. The Tauride accretionary orogen consists of upper crustal continent-  
468 derived nappes stacked below ophiolites that formed in late Cretaceous to Eocene time,  
469 during continental subduction below oceanic lithosphere (McPhee et al., 2018; van  
470 Hinsbergen et al., 2020) (Figure 3). During such thrusting, which is widespread across  
471 the Mediterranean orogens, the Greater Adriatic lithosphere that underpinned these  
472 nappes subducted (Jolivet and Brun, 2010; van Hinsbergen et al., 2005; van Hinsbergen  
473 and Schouten, 2021). The recognition of ~80 Ma old high-temperature, low-pressure  
474 deformation in the accreted continental Tauride nappes of the East Anatolian Plateau  
475 (Topuz et al., 2017) also suggests that the lithosphere was already thinned during that

476 time. After stacking of the nappes, the orogen was extended until the Eo-Oligocene, to  
477 form e.g. the Maden and Mut Basins (Aktaş and Robertson, 1984; Hüsing et al., 2009;  
478 Robertson et al., 2007) and leading to widespread extensional exhumation and crustal  
479 thinning (Küşçü et al., 2010; van Hinsbergen et al., 2020). Consequently, there was no  
480 mantle lithosphere to delaminate below the East Anatolian Plateau in the Miocene,  
481 making the loss of a lithospheric root an unlikely cause of late Neogene uplift.

482         Instead, our reconstruction shows that crustal thickening and shortening must  
483 have of played a far more important role in developing the high plateau of eastern  
484 Anatolia. This shortening component of ~200 km is similar to the width of the East  
485 Anatolian Plateau around Karlıova, which could thus have been shortened by ~50%  
486 since the onset of formation of the North Anatolian Fault. Such late Neogene shortening  
487 also explains how the modern crustal thickness: it is unlikely that the eastern Anatolian  
488 crust was 45 km thick during the depositio of its widespread lower to upper Miocene  
489 sedimentary cover (Gülyüz et al., 2020; Legeay et al., 2019; Şengör et al., 2008;  
490 Yusufoglu, 2013).

491         The onset of this shortening predates the onset of extrusion, both in the Sivas  
492 Basin and its eastern continuation (Legeay et al., 2019) and in the Bitlis Massif (Cavazza  
493 et al., 2018) and may even predate the arrival of the Arabian margin in the trench below  
494 the Tauride orogen (Figure 3). For both eastern Anatolia as well as the Caucasus  
495 (Cowgill et al., 2016; Vincent et al., 2007), the onset of upper plate shortening may well  
496 relate to the dynamics of the subduction zones involved, but similar to many other  
497 orogens (e.g. the Andes, pre-Cenozoic Tibet), the onset of upper plate shortening is not  
498 correlated with collision (van Hinsbergen and Schouten, 2021). From the available  
499 evidence, we do not see a direct causal relationship in space and time between the  
500 arrival of the Arabian Plate in the trench ('collision') and the onset of extrusion and  
501 microplate formation. Rather, Anatolian extrusion and the formation of the modern  
502 microplate developed gradually, accelerating over time, in a progressively rotating,  
503 shortening, and thickening orogenic belt that originated in the upper plate of a complex,  
504 long-lived subduction system, and that after the last phase of slab break-off was caught  
505 in between converging continents. The regional counterclockwise rotation of the  
506 eastern Tauride Orogen gradually changed the orientation of its pre-existing weakness  
507 zones through time, which may underpin the activation and abandonment of fault

508 segments throughout the transition period, and the ultimate eastward stepping of the  
509 Anatolian 'plate boundary' to the East Anatolian Fault in the Pliocene.

510 Finally, it is disconcerting that as much as 200 km of 'post-collisional'  
511 convergence appears challenging to identify in the geological record, for this indicates  
512 that we may be overlooking such shortening in orogens elsewhere where detailed  
513 balanced cross sections are lacking. Identifying how and where this shortening was and  
514 is being accommodated requires new, detailed field studies of the structures cutting and  
515 flanking the eastern Tauride Orogen. The lack of a connected mosaic of surface traces of  
516 the thrust faults across the plateau suggests that many of them are blind, buried below  
517 the widespread volcanic cover, calling for detailed and integrated geomorphological,  
518 geophysical, and geological field studies. The structures accommodating this  
519 convergence, even if blind, may still be active or reactivated and pose considerable  
520 seismic risk, as illustrated by the devastating, thrust-related October 23, 2011  $M_w$  7.1  
521 Van earthquake (Fielding et al., 2013). The detailed, integrated study of the structure  
522 and tectonic history of the East Anatolian Plateau will offer key insights into the  
523 dynamics and hazards of the East Anatolian Plateau tectonic hotspot.

524

## 525 Conclusions

526 The Anatolian microplate is widely considered a more or less rigid continental block,  
527 whose westward motion away from the Arabia-Eurasia collision zone causes  
528 devastating earthquakes, including those on February 6, 2023 along the East Anatolian  
529 Fault. How and why this microplate came into existence is important to evaluate the  
530 drivers of its motion and the assessment of associated seismic hazards. Here, we show a  
531 kinematic reconstruction of the Neogene evolution of the eastern Anatolian orogen, cast  
532 into a longer-term restoration of orogenic evolution since the Mesozoic. We review  
533 available constraints on fault motions and vertical axis rotations. These show that with  
534 the maximum estimates for displacement of Anatolia along the North Anatolian Fault,  
535 extrusion cannot account for more than 65 km (i.e. ~25%) of the total of 275 km of  
536 Arabia-Eurasia convergence since the onset of extrusion, 13 Ma ago. The remainder of  
537 convergence must have been accommodated by crustal shortening and thickening. We  
538 use our reconstruction to identify where this shortening may have been accommodated,  
539 but we stress that detailed, integrated geological, geophysical, and geomorphological

540 field studies are required to identify where and in what fashion this convergence was  
541 geologically accommodated. We postulate that orogenic shortening was likely the main  
542 driver of East Anatolian Plateau rise. The orogen that underlies the plateau likely  
543 already lost its lithospheric underpinnings during Cretaceous to Cenozoic orogenesis,  
544 making delamination and dynamic topographic rise a less likely contributor to plateau  
545 rise. Finally, we stress that detailed field studies are urgent in identifying the young  
546 orogenic history, and that structures accommodating orogenic shortening may still pose  
547 seismic hazards, besides the well-known hazards of Anatolia's prominent strike-slip  
548 system.

549

## 550 Acknowledgements

551

552 DJJvH acknowledges NWO VICI grant 865.17.001.

553

554

555 Figure captions

556

557 **Figure 1:** Anatolian Microplate within the framework of the major plates around the  
558 eastern Mediterranean region. AT = Aegean Trench; CT = Cyprus Trench; EAFZ = East  
559 Anatolian Fault Zone; NAFZ = North Anatolian Fault.

560

561 **Figure 2:** Detailed geological map, modified after the Geological Map of Turkey (Şenel,  
562 2002). Abbreviations: AB = Adana Basin; ATJ = Amik Triple Junction; BM = Bitlis Massif;  
563 BS = Bitlis Suture; EAFZ = East Anatolian Fault Zone; HB = Hakkari Basin; IAS = İzmir-  
564 Ankara Suture; NAFZ = North Anatolian Fault Zone; PM = Pötürge Massif; SB = Sivas  
565 Basin; SF = Sürgü Fault; KKS = Kağızman-Khoy Suture; KTJ = Karlıova Triple Junction;  
566 LV = Lake Van; MB = Maden Basin; MOF = Malatya-Ovacık Fault; MuB = Muş Basin; GF =  
567 Göksün Fault; KB = Kahramanmaraş Basin; VFZ = Varto Fault Zone; YGF = Yeşilgöz-  
568 Göksün Fault;

569

570 **Figure 3:** Paleo-tectonic maps of the Eastern Mediterranean region at selected time  
571 slices at a) 100 Ma, corresponding to the period of subduction initiation at an intra-  
572 Neotethyan subduction zone whose remains are widespread on the Anatolian Plateau  
573 ophiolites and associated mélangé; b) 85 Ma, corresponding to the time window of  
574 invasion by roll-back of intra-oceanic subduction zones into the Eastern Mediterranean,  
575 culminating in multidirectional ophiolite emplacement onto the Greater Adriatic and  
576 Arabian-north African continental margin; c) 65 Ma, corresponding to the end of  
577 ophiolite obduction, arrest of subduction in the Eastern Mediterranean Ocean, break-off  
578 of the associated slabs, and continuation of the northern originally intra-oceanic  
579 subduction zone by continental subduction and nappe stacking of the Greater Adria  
580 continent and overlying ophiolites; d) 45 Ma, corresponding to the time period of upper  
581 plate extension of the crust that now forms the East Anatolian Plateau, above the Bitlis  
582 subduction zone, whilst subduction below the Eurasian margin continues; e) 20 Ma,  
583 corresponding to the time window of upper plate shortening in eastern Anatolia, and  
584 the thrusting of the Tauride orogen over the Arabian margin; and f) the Present. Maps  
585 are based on the kinematic reconstruction of the Mediterranean region of van  
586 Hinsbergen et al. (2020). For key to the main units, see Figure 2.

587

588 **Figure 4.** Major active faults and epicenter of earthquakes ( $M_w \geq 5$ ) in Eastern Turkey.  
589 Focal mechanism solutions are provided by AFAD (Ministry of Interior Disaster and  
590 Emergency Management Presidency) and their locations are indicated with red dots  
591 with numbers. White dots represent the location of the earthquakes provided by the  
592 USGS (United States Geological Survey). The base map utilizes a Digital Elevation Model  
593 (DEM) provided by ASTER GDEM, with a horizontal resolution of 1 arc-second.

594

595 **Figure 5:** Simplified kinematic cartoon illustrating that the estimated amount of  
596 Anatolian extrusion of 85 km along the North Anatolian Fault since 13 Ma  
597 accommodates more than  $\sim 65$  km of Arabia-Europe convergence,  $\sim 25\%$ . The  
598 remaining  $>200$  km of convergence must have been accommodated by crustal  
599 shortening and thickening, uplifting the East Anatolian Plateau.

600

601 **Figure 6:** Paleo-tectonic maps of the East Anatolian Plateau. For clarity, the widespread  
602 ophiolite klippen, plutons, and sedimentary cover has been removed from the maps.  
603 Time slice at a) 18 Ma, corresponds to the time of onset of thrusting of the Tauride  
604 orogen over the Arabian margin; b) 13 Ma, corresponds to the onset of formation of the  
605 North Anatolian Fault; c) 5 Ma, corresponds to the onset of formation of the East  
606 Anatolian Fault, and d) corresponds to the Present. Maps are based on the kinematic  
607 reconstruction of the Mediterranean region of van Hinsbergen et al. (2020). BM = Bitlis  
608 Massif; CT = Cyprus Trench; Cy = Cyprus; EAFZ = East Anatolian Fault Zone; GF =  
609 Göksün Fault; KB = Kahramanmaraş Basin; MOF = Malatya-Ovacık Fault; NAFZ = North  
610 Anatolian Fault Zone; SB = Sivas Basin; SF = Sürgü Fault

611 For key to the main units, see Figure 2.

612

613

## 614 **References**

- 615 Akbayram, K., Sorlien, C.C., Okay, A.I., 2016. Evidence for a minimum  $52 \pm 1$  km of total  
616 offset along the northern branch of the North Anatolian Fault in northwest Turkey.  
617 *Tectonophysics* 668-669, 35-41.
- 618 Aktaş, G., Robertson, A., 1984. The Maden Complex, SE Turkey: evolution of a  
619 Neotethyan active margin. *Geological Society, London, Special Publications* 17, 375-  
620 402.
- 621 Balkaya, M., Ozden, S., Akyüz, H.S., 2021. Morphometric and Morphotectonic  
622 characteristics of Sürgü and Çardak Faults (East Anatolian Fault Zone). *Journal of*  
623 *Advanced Research in Natural and Applied Sciences* 7, 375-392.



624 Barazangi, M., Sandvol, E., Seber, D., 2006. Structure and tectonic evolution of the  
625 Anatolian plateau in eastern Turkey. *Geological Society of America Special Paper*  
626 409, 463-473.

627 Barbot, S., Luo, H., Wang, T., Hamiel, Y., Piatibratova, O., Javed, M.T., Braitenberg, C.,  
628 Gurbuz, G., 2023. Slip distribution of the February 6, 2023 Mw 7.8 and Mw 7.6,  
629 Kahramanmaraş, Turkey earthquake sequence in the East Anatolian Fault Zone.  
630 *Seismica* 2.

631 Brun, J.P., Sokoutis, D., 2010. 45 m.y. of Aegean crust and mantle flow driven by trench  
632 retreat. *Geology* 38, 815-818.

633 Buiter, S.J., Govers, R., Wortel, M., 2002. Two-dimensional simulations of surface  
634 deformation caused by slab detachment. *Tectonophysics* 354, 195-210.

635 Cavazza, W., Cattò, S., Zattin, M., Okay, A.I., Reiners, P., 2018. Thermochronology of the  
636 Miocene Arabia-Eurasia collision zone of southeastern Turkey. *Geosphere* 14, 2277-  
637 2293.

638 Cinku, M.C., 2017. Paleomagnetic results from Northeast Anatolia: remagnetization in  
639 Late Cretaceous sandstones and tectonic rotation at the Eastern extension of the  
640 Izmir-Ankara-Erzincan suture zone. *Acta Geophysica* 65, 1095-1109.

641 Cinku, M.C., Heller, F., Ustaömer, T., 2017. New paleomagnetic results from Upper  
642 Cretaceous arc-type rocks from the northern and southern branches of the  
643 Neotethys ocean in Anatolia. *International Journal of Earth Sciences* 106, 2575-  
644 2592.

645 Cowgill, E., Forte, A.M., Niemi, N., Avdeev, B., Tye, A., Trexler, C., Javakhishvili, Z.,  
646 Elashvili, M., Godoladze, T., 2016. Relict basin closure and crustal shortening  
647 budgets during continental collision: An example from Caucasus sediment  
648 provenance. *Tectonics* 35, 2918-2947.

649 DeMets, C., Iaffaldano, G., Merkouriev, S., 2015. High-resolution Neogene and  
650 Quaternary estimates of Nubia-Eurasia-North America Plate motion. *Geophysical*  
651 *Journal International* 203, 416-427.

652 DeMets, C., Merkouriev, S., 2016. High-resolution estimates of Nubia-Somalia plate  
653 motion since 20 Ma from reconstructions of the Southwest Indian Ridge, Red Sea  
654 and Gulf of Aden. *Geophysical Journal International* 207, 317-332.

655 Dewey, J., Şengör, A.M.C., 1979. Aegean and surrounding regions: complex multiplate  
656 and continuum tectonics in a convergent zone. *Geological Society of America*  
657 *Bulletin* 90, 84-92.

658 Duman, T.Y., Elmacı, H., Özalp, S., Kürçer, A., Kara, M., Özdemir, E., Yavuzoğlu, A., Uygun  
659 Gündoğan, Ç., 2020. Paleoseismology of the western Sürgü-Misis fault system: east  
660 Anatolian Fault, Turkey. *Mediterranean Geoscience Reviews* 2, 411-437.

661 Duman, T.Y., Emre, Ö., 2013. The East Anatolian Fault: geometry, segmentation and jog  
662 characteristics. *Geological Society, London, Special Publications* 372, SP372. 314.

663 Emre, Ö., Duman, T.Y., Özalp, S., Şaroğlu, F., Olgun, Ş., Elmacı, H., Çan, T., 2018. Active  
664 fault database of Turkey. *Bulletin of Earthquake Engineering* 16, 3229-3275.

665 Faccenna, C., Bellier, O., Martinod, J., Piromallo, C., Regard, V., 2006. Slab detachment  
666 beneath eastern Anatolia: A possible cause for the formation of the North Anatolian  
667 fault. *Earth and Planetary Science Letters* 242, 85-97.

668 Fielding, E.J., Lundgren, P.R., Taymaz, T., Yolsal-Çevikbilen, S., Owen, S.E., 2013. Fault-  
669 slip source models for the 2011 M 7.1 Van earthquake in Turkey from SAR  
670 interferometry, pixel offset tracking, GPS, and seismic waveform analysis.  
671 *Seismological Research Letters* 84, 579-593.

672 Göğüş, O.H., Pysklywec, R.N., 2008. Mantle lithosphere delamination driving plateau  
673 uplift and synconvergent extension in eastern Anatolia. *Geology* 36, 723-726.

674 Gülyüz, E., Durak, H., Özkaptan, M., Krijgsman, W., 2020. Paleomagnetic constraints on  
675 the early Miocene closure of the southern Neo-Tethys (Van region; East Anatolia):  
676 Inferences for the timing of Eurasia- Arabia collision. *Global and Planetary Change*  
677 185, 103089.

678 Gürer, D., van Hinsbergen, D.J.J., 2019. Diachronous demise of the Neotethys Ocean as a  
679 driver for non-cylindrical orogenesis in Anatolia. *Tectonophysics* 760, 95-106.

680 Gürer, D., van Hinsbergen, D.J.J., Matenco, L., Corfu, F., Cascella, A., 2016. Kinematics of a  
681 former oceanic plate of the Neotethys revealed by deformation in the Ulukışla basin  
682 (Turkey). *Tectonics* 35, 2385-2416.

683 Gürer, D., van Hinsbergen, D.J.J., Özkaptan, M., Creton, I., Koymans, M.R., Cascella, A.,  
684 Langereis, C.G., 2018. Paleomagnetic constraints on the timing and distribution of  
685 Cenozoic rotations in Central and Eastern Anatolia. *Solid Earth* 9, 295-322.

686 Hafkenscheid, E., Wortel, M.J.R., Spakman, W., 2006. Subduction history of the Tethyan  
687 region derived from seismic tomography and tectonic reconstructions. *Journal of*  
688 *Geophysical Research* 111.

689 Higgins, M., Schoenbohm, L.M., Brocard, G., Kaymakçı, N., Gosse, J.C., Cosca, M.A., 2015.  
690 New kinematic and geochronologic evidence for the Quaternary evolution of the  
691 Central Anatolian fault zone (CAFZ). *Tectonics* 34, 2118-2141.

692 Hubert-Ferrari, A., King, G., Woerd, J.v.d., Villa, I., Altunel, E., Armijo, R., 2009. Long-term  
693 evolution of the North Anatolian Fault: new constraints from its eastern  
694 termination. *Geological Society, London, Special Publications* 311, 133-154.

695 Hubert-Ferrari, A., Armijo, R., King, G., Meyer, B., Barka, A., 2002. Morphology,  
696 displacement, and slip rates along the North Anatolian Fault, Turkey. *Journal of*  
697 *Geophysical Research: Solid Earth* 107, ETG-9.

698 Hüsing, S.K., Zachariasse, W.-J., van Hinsbergen, D.J.J., Krijgsman, W., Inceöz, M.,  
699 Harzhauser, M., Mandic, O., Kroh, A., 2009. Oligocene–Miocene basin evolution in SE  
700 Anatolia, Turkey: constraints on the closure of the eastern Tethys gateway.  
701 *Geological Society, London, Special Publications* 311, 107-132.

702 Huvaz, O., 2009. Comparative petroleum systems analysis of the interior basins of  
703 Turkey: Implications for petroleum potential. *Marine and Petroleum Geology* 26,  
704 1656-1676.

705 Jaffey, N., Robertson, A.H., 2001. New sedimentological and structural data from the  
706 Ecemiş Fault Zone, southern Turkey: implications for its timing and offset and the  
707 Cenozoic tectonic escape of Anatolia. *Journal of the Geological Society* 158, 367-378.

708 Jolivet, L., Brun, J.-P., 2010. Cenozoic geodynamic evolution of the Aegean. *International*  
709 *Journal of Earth Sciences* 99, 109-138.

710 Kapp, P., Guynn, J.H., 2004. Indian punch rifts Tibet. *Geology* 32.

711 Karaoğlu, Ö., Selçuk, A.S., Gudmundsson, A., 2017. Tectonic controls on the Karlıova  
712 triple junction (Turkey): Implications for tectonic inversion and the initiation of  
713 volcanism. *Tectonophysics* 694, 368-384.

714 Kaymakçı, N., Inceöz, M., Ertepinar, P., Koç, A., 2010. Late Cretaceous to Recent  
715 kinematics of SE Anatolia (Turkey). *Geological Society, London, Special Publications*  
716 340, 409-435.

717 Keskin, M., 2003. Magma generation by slab steepening and breakoff beneath a  
718 subduction-accretion complex: An alternative model for collision-related volcanism  
719 in Eastern Anatolia, Turkey. *Geophysical Research Letters* 30.

720 Ketin, I., 1948. Über die tektonisch-mechanischen Folgerungen aus den grossen  
721 anatolischen Erdbeben des letzten Dezenniums. *Geologische Rundschau* 36, 77-83.

722 Koç, A., Kaymakcı, N., 2013. Kinematics of Sürgü Fault Zone (Malatya, Turkey): A remote  
723 sensing study. *Journal of Geodynamics* 65, 292-307.

724 Koçyiğit, A., Beyhan, A., 1998. A new intracontinental transcurrent structure: the Central  
725 Anatolian Fault Zone, Turkey. *Tectonophysics* 284, 317-336.

726 Koçyiğit, A., Yılmaz, A., Adamia, S., Kuloshvili, S., 2001. Neotectonics of East Anatolian  
727 Plateau (Turkey) and Lesser Caucasus: implication for transition from thrusting to  
728 strike-slip faulting. *Geodinamica Acta* 14, 177-195.

729 Küşçü, İ., Kuscu, G.G., Tosdal, R.M., Ulrich, T.D., Friedman, R., 2010. Magmatism in the  
730 southeastern Anatolian orogenic belt: transition from arc to post-collisional setting  
731 in an evolving orogen. *Geological Society, London, Special Publications* 340, 437-  
732 460.

733 Küşçü, İ., Tosdal, R.M., Gencalioglu-Kuşcu, G., Friedman, R., Ullrich, T.D., 2013. Late  
734 Cretaceous to Middle Eocene magmatism and metallogeny of a portion of the  
735 Southeastern Anatolian orogenic belt, East-Central Turkey. *Economic Geology* 108,  
736 641-666.

737 Le Pichon, X., Kreemer, C., 2010. The Miocene-to-Present Kinematic Evolution of the  
738 Eastern Mediterranean and Middle East and Its Implications for Dynamics. *Annual*  
739 *Review of Earth and Planetary Sciences* 38, 323-351.

740 Lefebvre, C., Meijers, M.J.M., Kaymakcı, N., Peynircioğlu, A., Langereis, C.G., van  
741 Hinsbergen, D.J.J., 2013. Reconstructing the geometry of central Anatolia during the  
742 late Cretaceous: Large-scale Cenozoic rotations and deformation between the  
743 Pontides and Taurides. *Earth and Planetary Science Letters* 366, 83-98.

744 Legeay, E., Ringenbach, J.-C., Kergaravat, C., Pichat, A., Mohn, G., Vergés, J., Kavak, K.S.,  
745 Callot, J.-P., 2019. Structure and kinematics of the Central Sivas Basin (Turkey): Salt  
746 deposition and tectonics in an evolving fold-and-thrust belt. *Geological Society,*  
747 *London, Special Publications* 490, SP490-2019-2092.

748 Li, S., Advokaat, E.L., van Hinsbergen, D.J.J., Koymans, M., Deng, C., Zhu, R., 2017.  
749 Paleomagnetic constraints on the Mesozoic-Cenozoic paleolatitudinal and rotational  
750 history of Indochina and South China: Review and updated kinematic  
751 reconstruction. *Earth-Science Reviews* 171, 58-77.

752 Liu, C., Lay, T., Wang, R., Taymaz, T., Xie, Z., Xiong, X., Irmak, T.S., Kahraman, M., Erman,  
753 C., 2023. Complex multi-fault rupture and triggering during the 2023 earthquake  
754 doublet in southeastern Türkiye. *Nat Commun* 14, 5564.

755 Maffione, M., van Hinsbergen, D.J.J., de Gelder, G.I.N.O., van der Goes, F.C., Morris, A.,  
756 2017. Kinematics of Late Cretaceous subduction initiation in the Neo-Tethys Ocean  
757 reconstructed from ophiolites of Turkey, Cyprus, and Syria. *Journal of Geophysical*  
758 *Research: Solid Earth* 122, 3953-3976.

759 Mann, P., Taylor, F., Edwards, R.L., Ku, T.-L., 1995. Actively evolving microplate  
760 formation by oblique collision and sideways motion along strike-slip faults: An  
761 example from the northeastern Caribbean plate margin. *Tectonophysics* 246, 1-69.

762 McKenzie, D.P., Parker, R.L., 1967. The North Pacific: an example of tectonics on a  
763 sphere. *Nature* 216, 1276-1280.

764 McPhee, P.J., Altner, D., van Hinsbergen, D.J.J., 2018. First Balanced Cross Section Across  
765 the Taurides Fold-Thrust Belt: Geological Constraints on the Subduction History of  
766 the Antalya Slab in Southern Anatolia. *Tectonics*.

767 McPhee, P.J., Koç, A., van Hinsbergen, D.J.J., 2022. Preparing the ground for plateau  
768 growth: Late Neogene Central Anatolian uplift in the context of orogenic and  
769 geodynamic evolution since the Cretaceous. *Tectonophysics* 822, 229131.

770 McPhee, P.J., van Hinsbergen, D.J.J., 2019. Tectonic reconstruction of Cyprus reveals Late  
771 Miocene continental collision between Africa and Anatolia. *Gondwana Research* 68,  
772 158-173.

773 Melgar, D., Taymaz, T., Ganas, A., Crowell, B.W., Öcalan, T., Kahraman, M., Tsironi, V.,  
774 Yolsal-Çevikbil, S., Valkaniotis, S., Irmak, T.S., 2023. Sub-and super-shear ruptures  
775 during the 2023 Mw 7.8 and Mw 7.6 earthquake doublet in SE Türkiye. *Seismica* 2,  
776 1-10.

777 Memiş, C., Göğüş, O.H., Uluocak, E.Ş., Pysklywec, R., Keskin, M., Şengör, A.C., Topuz, G.,  
778 2020. Long wavelength progressive plateau uplift in Eastern Anatolia since 20 Ma:  
779 implications for the role of slab peel-Back and Break-off. *Geochemistry, Geophysics,*  
780 *Geosystems* 21, e2019GC008726.

781 Molin, P., Sembroni, A., Ballato, P., Faccenna, C., 2023. The uplift of an early stage  
782 collisional plateau unraveled by fluvial network analysis and river longitudinal  
783 profile inversion: The case of the Eastern Anatolian Plateau. *Tectonics* 42.

784 Molnar, P., Tapponnier, P., 1975. Cenozoic tectonics of Asia: effects of a continental  
785 collision. *science* 189, 419-426.

786 Mueller, M., Licht, A., Campbell, C., Oçakoğlu, F., Taylor, M., Burch, L., Ugrai, T., Kaya, M.,  
787 Kurtoğlu, B., Coster, P., 2019. Collision chronology along the İzmir-Ankara-Erzincan  
788 suture zone: Insights from the Sarıcakaya Basin, western Anatolia. *Tectonics* 38,  
789 3652-3674.

790 Muñoz, J.A., 1992. Evolution of a continental collision belt: ECORS-Pyrenees crustal  
791 balanced cross-section, in: McClay, K.R. (Ed.), *Thrust Tectonics*. Springer  
792 Netherlands, Dordrecht, pp. 235-246.

793 Nikogosian, I.K., Bracco Gartner, A.J., Mason, P.R., van Hinsbergen, D.J.J., Kuiper, K.F.,  
794 Kirscher, U., Matveev, S., Grigoryan, A., Grigoryan, E., Israyelyan, A., 2023. The South  
795 Armenian Block: Gondwanan origin and Tethyan evolution in space and time.  
796 *Gondwana Research* 121, 168-195.

797 Nuriel, P., Craddock, J., Kylander-Clark, A.R., Uysal, I.T., Karabacak, V., Dirik, R.K., Hacker,  
798 B.R., Weinberger, R., 2019. Reactivation history of the North Anatolian fault zone  
799 based on calcite age-strain analyses. *Geology* 47, 465-469.

800 Oberhänsli, R., Candan, O., Wilke, F., 2010. Geochronological Evidence of Pan-African  
801 Eclogites from the Central Menderes Massif, Turkey. *Turkish Journal of Earth*  
802 *Sciences* 19, 431-447.

803 Oberhänsli, R., Koralay, E., Candan, O., Pourteau, A., Bousquet, R., 2014. Late Cretaceous  
804 eclogitic high-pressure relics in the Bitlis Massif. *Geodinamica Acta* 26, 175-190.

805 Oçakoğlu, F., Hakyemez, A., Açıkalın, S., Özkan Altınır, S., Büyükmeriç, Y., Licht, A.,  
806 Demircan, H., Şafak, Ü., Yıldız, A., Yılmaz, İ.Ö., 2019. Chronology of subduction and  
807 collision along the İzmir-Ankara suture in Western Anatolia: records from the  
808 Central Sakarya Basin. *International Geology Review* 61, 1244-1269.

809 Okay, A.I., Zattin, M., Cavazza, W., 2010. Apatite fission-track data for the Miocene  
810 Arabia-Eurasia collision. *Geology* 38, 35-38.

811 Philippon, M., Brun, J.-P., Gueydan, F., Sokoutis, D., 2014. The interaction between  
812 Aegean back-arc extension and Anatolia escape since Middle Miocene.  
813 *Tectonophysics* 631, 176-188.

814 Racano, S., Schildgen, T., Ballato, P., Yıldırım, C., Wittmann, H., 2023. Rock-uplift history  
815 of the Central Pontides from river-profile inversions and implications for

816 development of the North Anatolian Fault. *Earth and Planetary Science Letters* 616,  
817 118231.

818 Reilinger, R., McClusky, S., Vernant, P., Lawrence, S., Ergintav, S., Cakmak, R., Ozener, H.,  
819 Kadirov, F., Guliev, I., Stepanyan, R., Nadariya, M., Hahubia, G., Mahmoud, S., Sakr, K.,  
820 ArRajehi, A., Paradissis, D., Al-Aydrus, A., Prilepin, M., Guseva, T., Evren, E.,  
821 Dmitrotsa, A., Filikov, S.V., Gomez, F., Al-Ghazzi, R., Karam, G., 2006. GPS constraints  
822 on continental deformation in the Africa-Arabia-Eurasia continental collision zone  
823 and implications for the dynamics of plate interactions. *Journal of Geophysical*  
824 *Research: Solid Earth* 111, n/a-n/a.

825 Robertson, A., Parlak, O., Rizaoglu, T., Ünlügenç, Ü., İnan, N., Tasli, K., Ustaömer, T., 2007.  
826 Tectonic evolution of the South Tethyan ocean: evidence from the Eastern Taurus  
827 Mountains (Elazığ region, SE Turkey). *Geological Society, London, Special*  
828 *Publications* 272, 231-270.

829 Sakellariou, D., Tsampouraki-Kraounaki, K., 2019. Plio-Quaternary extension and strike-  
830 slip tectonics in the Aegean, Transform plate boundaries and fracture zones.  
831 Elsevier, pp. 339-374.

832 Sançar, T., Zabcı, C., Akcar, N., Karabacak, V., Yeşilyurt, S., Yazıcı, M., Akyüz, H.S., Önal,  
833 A.Ö., Ivy-Ochs, S., Christl, M., 2020. Geodynamic importance of the strike-slip faults  
834 at the eastern part of the Anatolian Scholle: Inferences from the uplift and slip rate  
835 of the Malatya Fault (Malatya-Ovacık Fault Zone, eastern Turkey). *Journal of Asian*  
836 *earth sciences* 188, 104091.

837 Sançar, T., Zabcı, C., Akyüz, H.S., Sunal, G., Villa, I.M., 2015. Distributed transpressive  
838 continental deformation: the Varto Fault Zone, eastern Turkey. *Tectonophysics* 661,  
839 99-111.

840 Sançar, T., Zabcı, C., Karabacak, V., Yazıcı, M., Akyüz, H.S., 2019. Geometry and  
841 Paleoseismology of the Malatya Fault (Malatya-Ovacık Fault Zone), Eastern Turkey:  
842 Implications for intraplate deformation of the Anatolian Scholle. *Journal of*  
843 *Seismology* 23, 319-340.

844 Saroğlu, F., 1992. The east Anatolian fault zone of Turkey. *Ann. Tectonicae*, 99-125.

845 Schepers, G., van Hinsbergen, D.J.J., Spakman, W., Kosters, M.E., Boschman, L.M.,  
846 McQuarrie, N., 2017. South-American plate advance and forced Andean trench  
847 retreat as drivers for transient flat subduction episodes. *Nat Commun* 8, 15249.

848 Şenel, M., 2002. Geological Map of Turkey in 1/500.000 scale. Publication of Mineral  
849 Research and Exploration Directorate of Turkey (MTA), Ankara.

850 Sengör, A., 1979. The North Anatolian transform fault: its age, offset and tectonic  
851 significance. *Journal of the Geological Society* 136, 269-282.

852 Şengör, A.M.C., Özeren, M., Genç, T., Zor, E., 2003. East Anatolian High Plateau as a  
853 mantle-supported, north-south shortened domal structure. *Geophysical Research*  
854 *Letters* 30, 8050.

855 Şengör, A.M.C., Özeren, M.S., Keskin, M., Sakıncı, M., Özbakır, A.D., Kayan, İ., 2008. Eastern  
856 Turkish high plateau as a small Turkic-type orogen: Implications for post-collisional  
857 crust-forming processes in Turkic-type orogens. *Earth-Science Reviews* 90, 1-48.

858 Şengör, A.M.C., Tüysüz, O., İmren, C., Sakıncı, M., Eyidoğan, H., Görür, N., Le Pichon, X.,  
859 Rangin, C., 2005. The North Anatolian Fault: A New Look. *Annual Review of Earth*  
860 *and Planetary Sciences* 33, 37-112.

861 Şengör, A.M.C., Yılmaz, Y., 1981. Tethyan evolution of Turkey: A plate tectonic approach.  
862 *Tectonophysics* 75, 181-241.

863 Simão, N., Nalbant, S.S., Sunbul, F., Mutlu, A.K., 2016. Central and eastern Anatolian  
864 crustal deformation rate and velocity fields derived from GPS and earthquake data.  
865 Earth and Planetary Science Letters 433, 89-98.

866 Sosson, M., Rolland, Y., Müller, C., Danelian, T., Melkonyan, R., Kekelia, S., Adamia, S.,  
867 Babazadeh, V., Kangarli, T., Avagyan, A., 2010. Subductions, obduction and collision  
868 in the Lesser Caucasus (Armenia, Azerbaijan, Georgia), new insights. Geological  
869 Society, London, Special Publications 340, 329-352.

870 Sternai, P., Jolivet, L., Menant, A., Gerya, T., 2014. Driving the upper plate surface  
871 deformation by slab rollback and mantle flow. Earth and Planetary Science Letters  
872 405, 110-118.

873 Tan, O., Tapirdamaz, M.C., Yörük, A., 2008. The earthquake catalogues for Turkey.  
874 Turkish Journal of Earth Sciences 17, 405-418.

875 Tari, U., Tüysüz, O., Can Genç, Ş., İmren, C., Blackwell, B.A., Lom, N., Tekeşin, Ö., Üsküplü,  
876 S., Erel, L., Altiok, S., 2013. The geology and morphology of the Antakya Graben  
877 between the Amik Triple Junction and the Cyprus Arc. Geodinamica Acta 26, 27-55.

878 Topuz, G., Candan, O., Zack, T., Yılmaz, A., 2017. East Anatolian plateau constructed over  
879 a continental basement: No evidence for the East Anatolian accretionary complex.  
880 Geology 45, 791-794.

881 van der Boon, A., van Hinsbergen, D.J.J., Rezaeian, M., Gürer, D., Honarmand, M., Pastor-  
882 Galán, D., Krijgsman, W., Langereis, C.G., 2018. Quantifying Arabia–Eurasia  
883 convergence accommodated in the Greater Caucasus by paleomagnetic  
884 reconstruction. Earth and Planetary Science Letters 482, 454-469.

885 van Hinsbergen, D.J.J., 2022. Indian Plate paleogeography, subduction, and horizontal  
886 underthrusting below Tibet: paradoxes, controversies, and opportunities. National  
887 Science Review 9, nwac074.

888 van Hinsbergen, D.J.J., Hafkenscheid, E., Spakman, W., Meulenkaamp, J.E., Wortel, R., 2005.  
889 Nappe stacking resulting from subduction of oceanic and continental lithosphere  
890 below Greece. Geology 33.

891 van Hinsbergen, D.J.J., Schmid, S.M., 2012. Map view restoration of Aegean-West  
892 Anatolian accretion and extension since the Eocene. Tectonics 31, n/a-n/a.

893 van Hinsbergen, D.J.J., Schouten, T.L.A., 2021. Deciphering paleogeography from  
894 orogenic architecture: constructing orogens in a future supercontinent as thought  
895 experiment. American Journal of Science 321, 955-1031.

896 van Hinsbergen, D.J.J., Torsvik, T., Schmid, S.M., Matenco, L., Maffione, M., Vissers, R.L.M.,  
897 Gürer, D., Spakman, W., 2020. Orogenic architecture of the Mediterranean region  
898 and kinematic reconstruction of its tectonic evolution since the Triassic. Gondwana  
899 Research 81, 79-229.

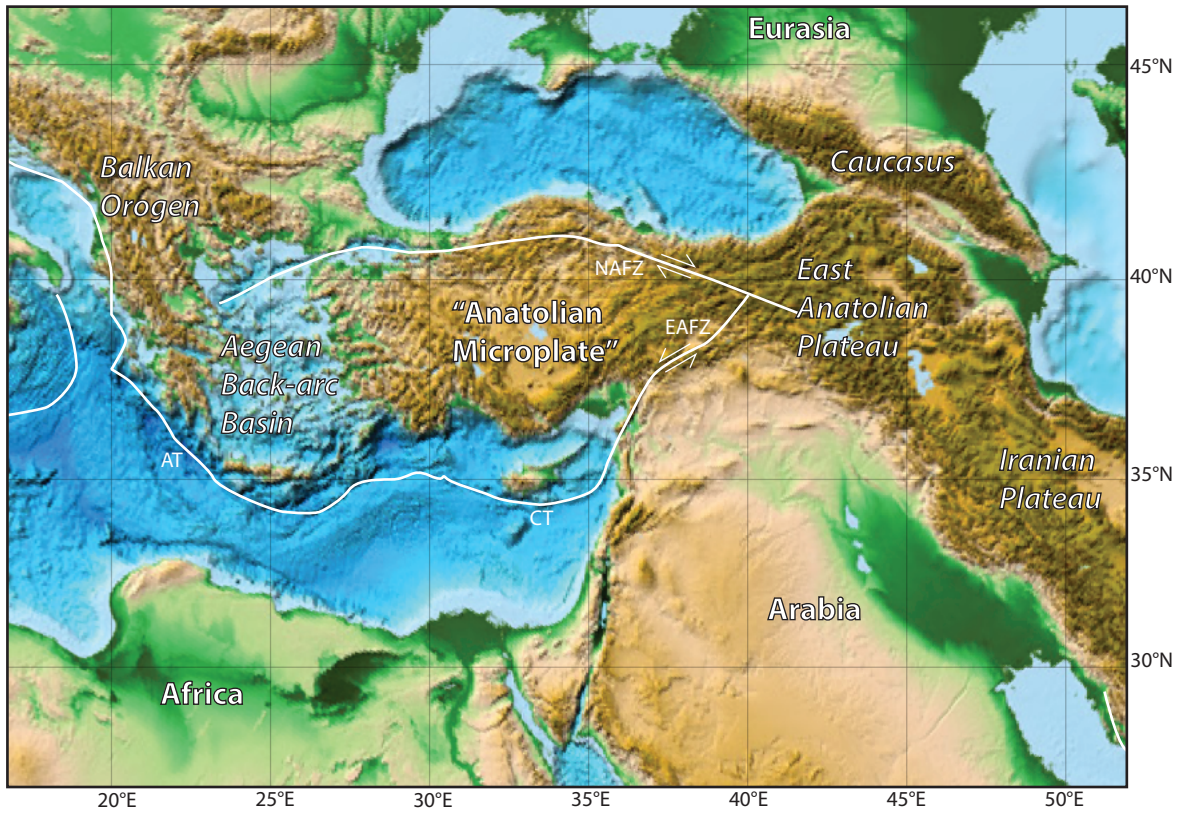
900 van Hinsbergen, D.J.J., van der Meer, D.G., Zachariasse, W.J., Meulenkaamp, J.E., 2006.  
901 Deformation of western Greece during Neogene clockwise rotation and collision  
902 with Apulia. International Journal of Earth Sciences 95, 463-490.

903 Vincent, S.J., Morton, A.C., Carter, A., Gibbs, S., Barabadze, T.G., 2007. Oligocene uplift of  
904 the Western Greater Caucasus: an effect of initial Arabia–Eurasia collision. Terra  
905 Nova 19, 160-166.

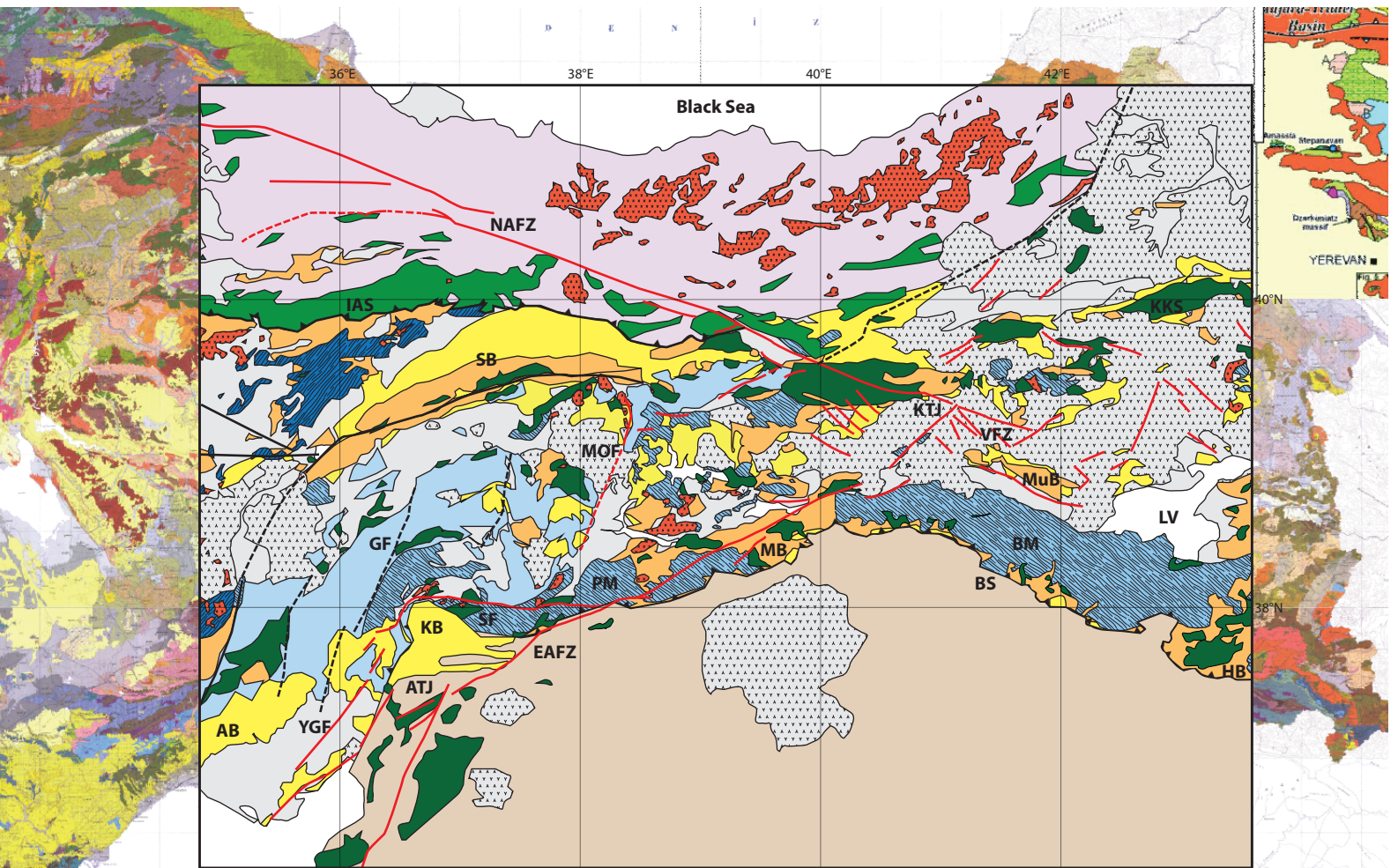
906 Westaway, R., 2004. Kinematic consistency between the Dead Sea Fault Zone and the  
907 Neogene and Quaternary left-lateral faulting in SE Turkey. Tectonophysics 391,  
908 203-237.
















909 Westaway, R., Arger, J., 2001. Kinematics of the Malatya–Ovacik fault zone. Geodinamica  
910 Acta 14, 103-131.

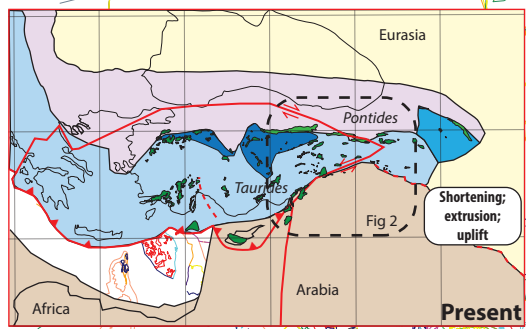
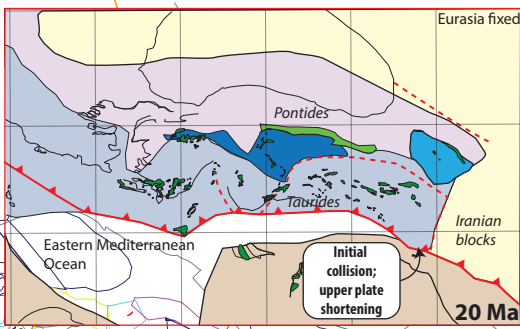
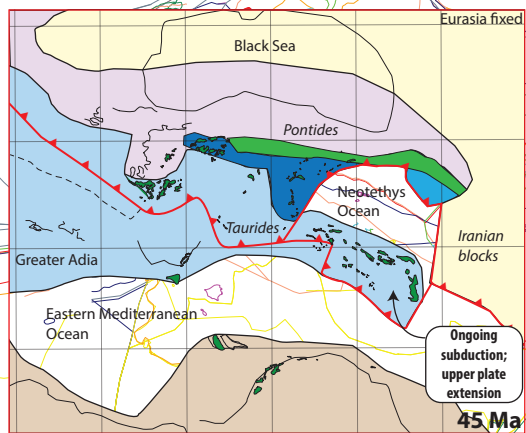
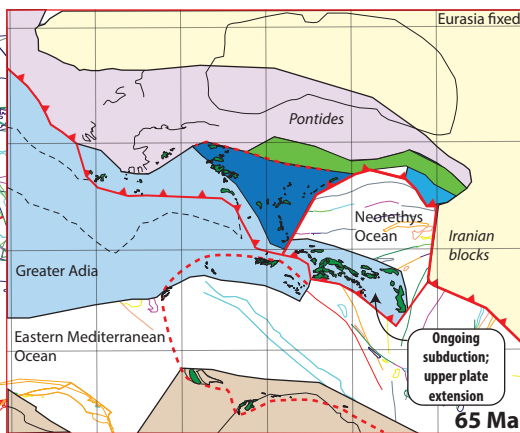
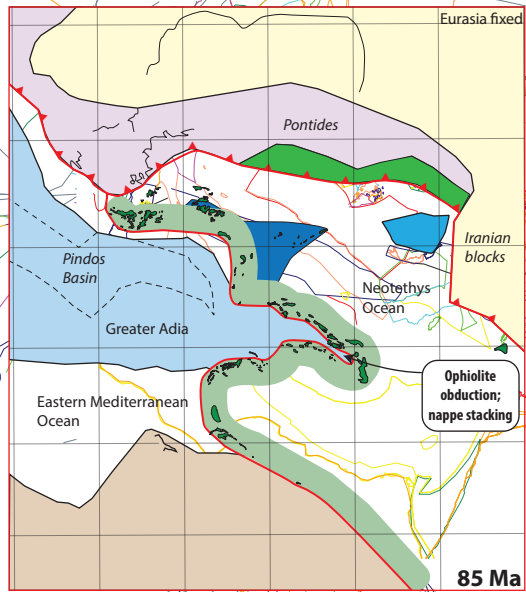
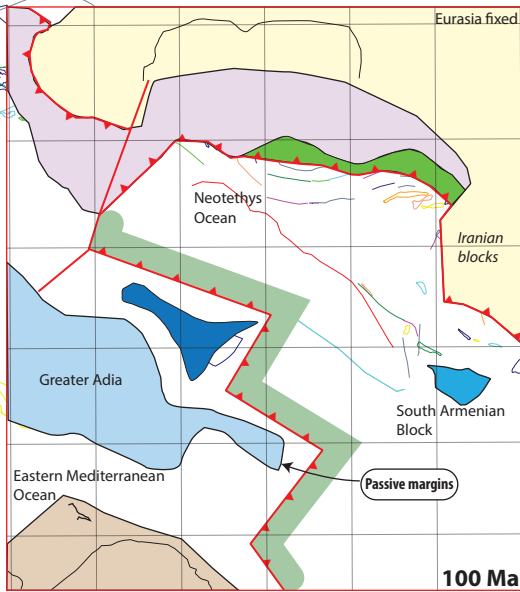
911 Whitney, D.L., Delph, J.R., Thomson, S.N., Beck, S.L., Brocard, G.Y., Cosca, M.A., Darin,  
912 M.H., Kaymakçı, N., Meijers, M.J., Okay, A.I., 2023. Breaking plates: Creation of the  
913 East Anatolian fault, the Anatolian plate, and a tectonic escape system. *Geology*.  
914 Yılmaz, O., Michel, R., Vialette, Y., Bonhomme, M., 1981. Réinterprétation des données  
915 isotopiques Rb-Sr obtenues sur les métamorphites de la partie méridionale du  
916 massif de Bitlis (Turquie). *Sciences Géologiques, bulletins et mémoires* 34, 59-73.  
917 Yönlü, Ö., Altunel, E., Karabacak, V., Akyüz, H.S., 2013. Evolution of the Gölbaşı basin and  
918 its implications for the long-term offset on the East Anatolian Fault Zone, Turkey.  
919 *Journal of Geodynamics* 65, 272-281.  
920 Yusufoglu, H., 2013. An intramontane pull-apart basin in tectonic escape deformation:  
921 Elbistan Basin, Eastern Taurides, Turkey. *Journal of Geodynamics* 65, 308-329.  
922 Zhang, Y., Tang, X., Liu, D., Taymaz, T., Eken, T., Guo, R., Zheng, Y., Wang, J., Sun, H., 2023.  
923 Geometric controls on cascading rupture of the 2023 Kahramanmaraş earthquake  
924 doublet. *Nature Geoscience*, 1-7.  
925 Zor, E., Sandvol, E., Gürbüz, C., Türkelli, N., Seber, D., Barazangi, M., 2003. The crustal  
926 structure of the East Anatolian plateau (Turkey) from receiver functions.  
927 *Geophysical Research Letters* 30.  
928



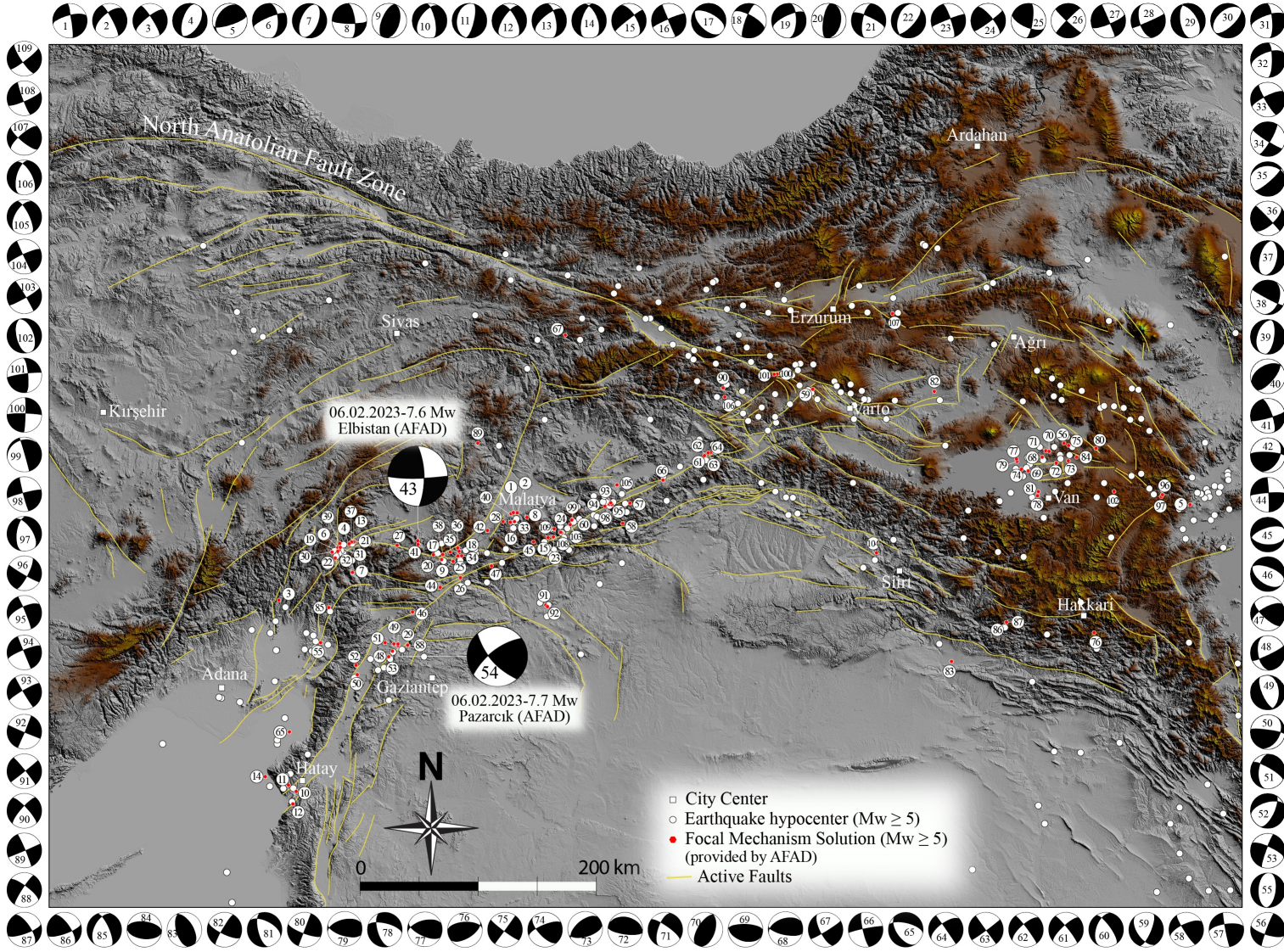


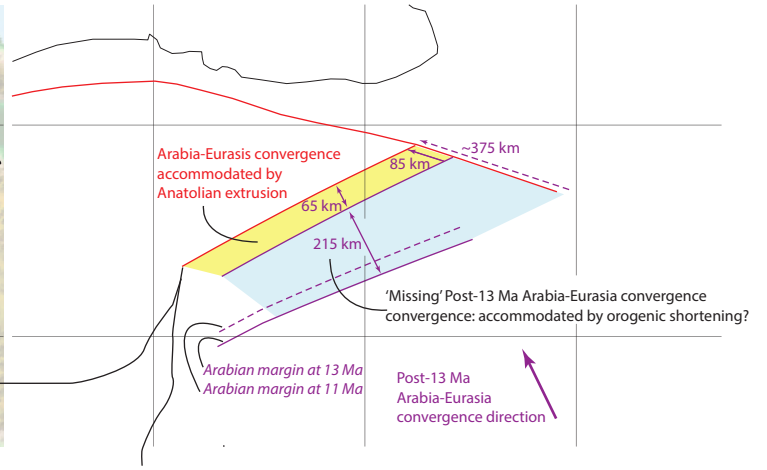
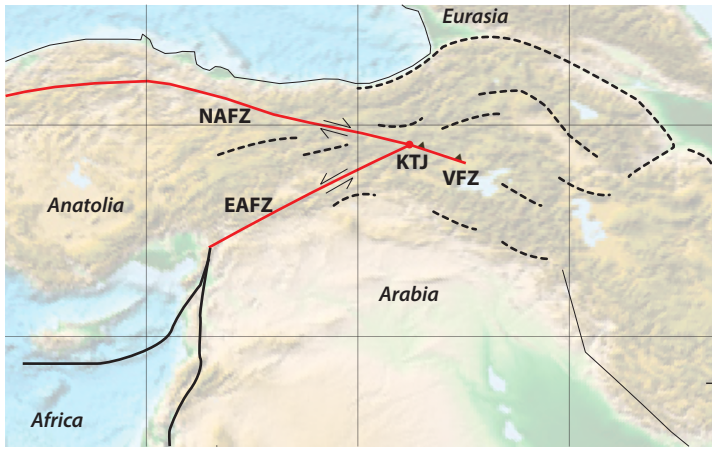


- |  |  |  |
|--|--|--|
|  Arabia                           |  Jurassic ophiolites          |  Upper Eocene-Oligocene sedimentary cover |
|  Pontides                         |  Cretaceous ophiolites        |  Miocene sedimentary cover                |
|  Non-metamorphosed Tauride nappes |  Cretaceous-Paleogene plutons |  Upper Neogene volcanic cover             |
|  Metamorphosed Tauride nappes     |  Active fault                 |  Plio-Quaternary sedimentary cover        |
|  Kırşehir Block                   |  Major inactive fault/suture  |  Sea/lake                                 |



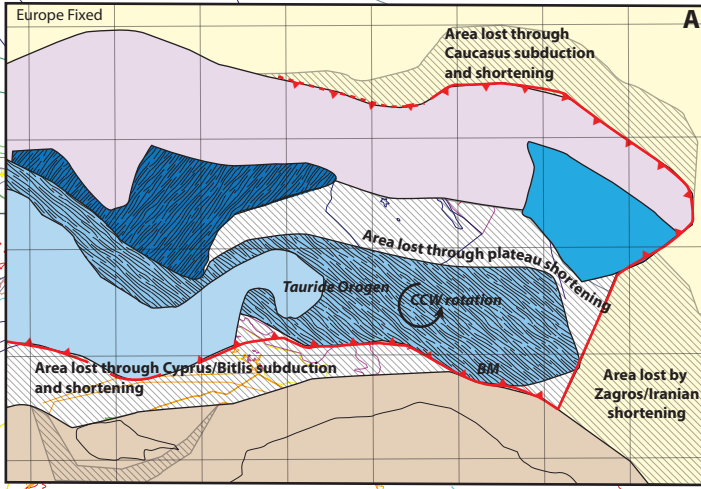




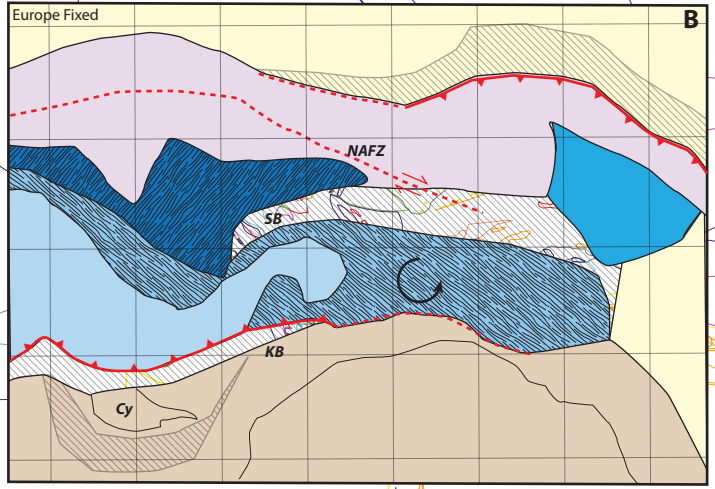




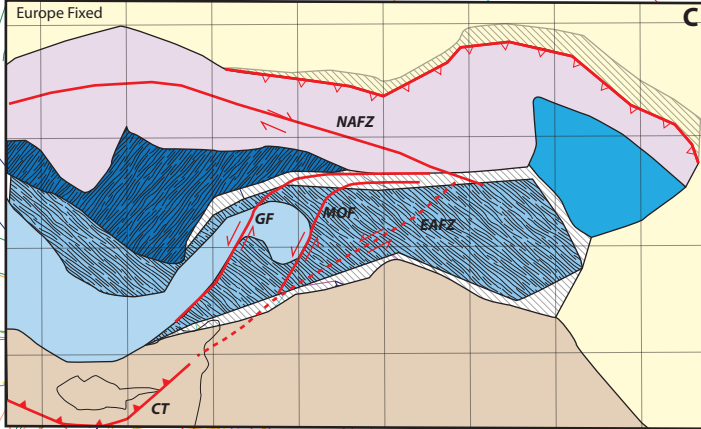
18 Ma: Initial thrusting of Tauride orogen over Arabian margin



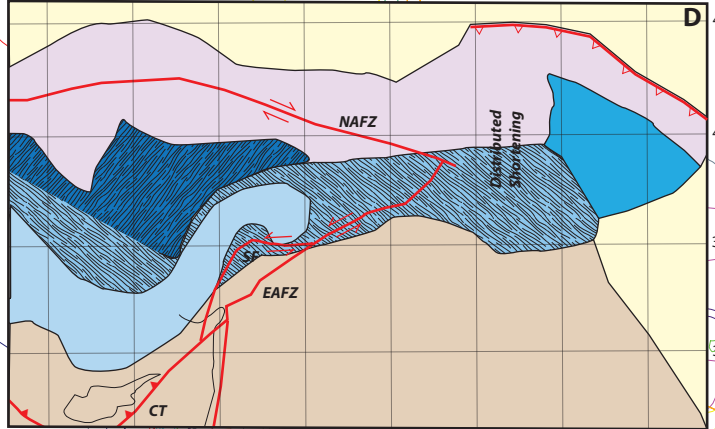
13 Ma: Onset of formation of the North Anatolian Fault



5 Ma: Onset of formation of the East Anatolian Fault



Present: microplate extrusion + distributed shortening



32°E 34°E 36°E 38°E 40°E 42°E 44°E 46°E

42°N  
40°N  
38°N  
36°N